Defence Technology 15 (2019) 146–153

Contents lists available at ScienceDirect

Defence Technology

journal homepage: www.elsevier.com/locate/dt

The detrimental effect of autofrettage on externally cracked modern tank gun barrels

M. Perl[*, 1, 2], T. Saley [1]

Pearlstone Center for Aeronautical Engineering Studies, Department of Mechanical Engineering, Ben-Gurion University of the Negev, Beer-Sheva, 84105, Israel

ARTICLE INFO

Article history:
Received 7 September 2018
Received in revised form
3 October 2018
Accepted 15 October 2018
Available online 16 October 2018

Keywords:
Gun barrel
Swage and hydraulic autofrettage
External crack
3-D
Finite element

ABSTRACT

Overstraining gun tubes has a twofold advantage. First, it enables the increase of the Safe Maximum Pressure (SMP) in the tube, resulting in a higher muzzle velocity which extends the gun's range and its projectile kinetic energy. Second, it reduces the tube's susceptibility to internal cracking which prolongs its fatigue life. Unfortunately, autofrettage also bears an inherent detrimental effect as it considerably increases the tensile hoop stress at the outer portion of the barrel's wall, which enhances external cracking of the tube by increasing the prevailing Stress Intensity Factor (SIF). In order to quantify this disadvantageous effect, 3-D Mode I SIFs distributions along the front of a single external radial semi-elliptical crack initiating from the outer surface of an autofrettaged modern gun barrel, overstrained by either the Swage or the Hydraulic autofrettage processes, are evaluated. The analysis is performed by the finite element (FE) method, using singular elements along the crack front. Innovative residual stress fields (RSFs), incorporating the Bauschinger effect for both types of autofrettage are applied to the barrel. Hill's [1] RSF is also applied to the tube for comparison reasons. All three RSFs are incorporated in the FE analysis, using equivalent temperature fields. Values for K_{IA} - the SIF resulting from the tensile residual stresses induced by autofrettage are evaluated for: a typical barrel of radii ratio $R_o/R_i = 2$, crack depth to wall-thickness ratios ($a/t = 0.005–0.1$), crack ellipticities ($a/c = 0.2–1.0$), and five levels of Swage, Hydraulic and Hill's autofrettage ($\varepsilon = 40\%$, 60%, 70%, 80%, and 100%). In total, 375 different 3-D cases are analyzed. The analysis demonstrates undoubtedly the detrimental effect of all types of autofrettage in increasing the prevailing effective stress intensity factor of external cracks, resulting in crack initiation enhancement and crack growth rate acceleration which considerably shortens the total fatigue life of the barrel. Nonetheless, the detrimental effect is autofrettage-type dependent. Swage and Hydraulic autofrettage RSFs differ substantially from each other. The disadvantageous effect of Swage autofrettage is much greater than that resulting from Hydraulic autofrettage. The results also emphasize the significance of the Bauschinger effect and the importance of the 3-D analysis.

1. Introduction

Gun barrels, as well as other cylindrical pressure vessels, have been autofrettaged for more than a hundred years in order to improve their operational performance. A favorable compressive residual hoop stress is induced at the gun's bore as a result of overstraining. This compressive stress at the tube's wall inner portion has a dual favorable effect. On the one hand, it enables to increases the allowable internal pressure in the tube, resulting in a higher muzzle velocity, which in turn extends the gun's range and its munitions kinetic energy. On the other hand, it reduces its susceptibility to internal cracking, which prolongs its fatigue life. At the same time, unfortunately, autofrettage also bears an inherent detrimental effect as it induces tensile residual hoop stresses at the outer portion of the barrel's wall, which boosts external cracking of the tube by increasing the prevailing Stress Intensity Factor (SIF) for cracks emanating from the outer surface of the barrel. Two processes are commonly used to overstrain gun barrels: Hydraulic autofrettage and Swage autofrettage. Both create similar patterns of

* Corresponding author.
E-mail address: merpr01@bgu.ac.il (M. Perl).
Peer review under responsibility of China Ordnance Society
[1] Aaron Fish Professor Emeritus of Mechanical Engineering-Fracture Mechanics and graduate student respectively.
[2] Fellow ASME.

https://doi.org/10.1016/j.dt.2018.10.001

Nomenclature

a	Crack depth
c	Crack half length
K_{00}	Normalizing SIF [eq. (1)]
K_I	Mode I SIF
K_{IA}	Mode I SIF due to autofrettage
$K_{IA\max}$	Maximum SIF due to autofrettage along crack front
K_{IN}	Combined SIF
$K_{IN\max}$	Maximum combined SIF
K_{IP}	Mode I SIF due to internal pressure
L	Cylinder's length
p	Internal pressure
R_i	Inner radius of the barrel
R_o	Outer radius of the barrel
r, θ, z	Cylindrical coordinates
t	Barrel's wall thickness

Greek Symbols

ε	Level of autofrettage
ν	Poisson's ratio
$\sigma_{\theta\theta}^{Res}$	Residual hoop stress component
σ_{rr}^{Res}	Residual radial stress component
σ_y	Initial yield stress
Φ	Parametric angle (Fig. 2(b))

Superscripts

Hill	Hill's autofrettage
Hyd	Hydraulic autofrettage (Perl and Perry 2006 [19])
Swage	Swage autofrettage (Perl and Perry 2006 [19])

Acronyms

DOF	Degrees of freedom
FEM	Finite element method
LEFM	Linear elastic fracture mechanics
MBT	Main Battle Tank
RSF	Residual stress field
SIF	Stress intensity factor

residual stress fields, yet of different distributions and magnitudes.

While the beneficial effect of realistic autofrettage has been thoroughly researched by among others Perl and Saley [2,3], the detrimental effect of overstraining has not been studied at all. For obvious mechanical reasons, the outer surface of barrels may bear functional geometrical discontinuities such as keyseats, grooves, part-through holes, etc., as well as scratches. Under operational conditions, the outer surface of the barrel is subjected to the cyclic action of high pressure pulses during firing, and is exposed to corrosive materials and an aggressive environment. The presence of the stress concentrators, the repeated loading and the corrosive environment may result in initiating one or a few 3-D, semi-elliptical radial cracks from the barrel's external surface into the barrel's wall. The largest of these cracks, commonly coined “the major crack”, which grows due to cyclic loading, may become critical, and cause catastrophic barrel failure.

The fatigue process of such cracks is governed by the prevailing combined Stress Intensity Factor (SIF) K_{IN} [3] which, in this case, consists of two components: K_{IP} - the SIF due to internal pressure, and K_{IA} - the positive SIF due to the tensile residual stresses induced by autofrettage i. e., $K_{IN} = K_{IP} + K_{IA}$. Several results are presently available for K_{IP} for external cracks in thick-walled cylindrical pressure vessels by, among others, Raju and Newman [4], Zheng et al. [5], Anderson [6] and Gerasimenko [7]. However, to the best of the authors knowledge, values for K_{IA} were never evaluated for external cracks in autofrettaged cylinders. It is, therefore, the purpose of the present analysis to evaluate K_{IA}, the ***positive*** SIF due to autofrettage, for a single external crack prevailing in an overstrained modern gun barrel applying an innovative, realistic, experimentally based autofrettage model, hereafter explained, which enables a very accurate replication of both Hydraulic and Swage autofrettage residual stress fields (RSFs) in a fully or partially overstrained barrel. For comparison reasons, Hill's [1] RSF is also applied. SIFs for a typical modern tank gun barrel of radii ratio $R_o/R_i = 2$, for crack depth to wall-thickness ratios ($a/t = 0.005–0.1$), crack ellipticities ($a/c = 0.2–1.0$), and five levels of Swage, Hydraulic and Hill's autofrettage ($\varepsilon = 40\%$, 60%, 70%, 80%, and 100%) are evaluated. This particular range of relative crack depth of $a/t = 0.005$ to 0.1 is chosen to enable the comparison with internal cracks [2].

2. Autofrettage and its simulation

There has been a continuous effort to increase the pressure carrying capacity of gun barrels aiming at extending their firing range since the 17th century. A new metal fabrication process was suggested to achieve this goal by a French Artillery officer Col. L. Jacob [8] at the beginning of the 20th century. Since that time, this process, known as autofrettage - self-hooping in French, has been used in gun barrel manufacturing, and in a variety of other cylindrical pressure vessel applications such as nuclear reactor vessels, high pressure oil field pipes, low-density polyethylene processing etc. The process of autofrettage, initially meant to enable an increase in the gun's internal pressure, was also found to reduce the gun's sensitivity to ***internal*** cracking, i.e., inhibiting crack initiation and moderating crack growth rate, thus extending remarkably the barrel's fatigue life.

The first process to be used for barrel overstraining was Hydraulic Autofrettage. In the first stage of this process, the tube is subjected to an increasing internal hydraulic pressure until plastic deformation onsets at the bore. As pressure is further increased, the plastic deformation progresses through the tube's wall until it reaches the outside surface and the barrel is then considered fully autofrettaged. In case the process is interrupted while the plastic deformation moved only through part of the tube's wall, the tube is only partially autofrettaged. In the second stage, the hydraulic pressure is released and elastic recovery occurs resulting in a residual stress field through the cylinder's wall. The residual hoop stress component is compressive at the inner portion of the tube's wall and tensile at its outer part. The largest residual compressive hoop stress occurs at the bore, and it monotonically changes into a residual tensile hoop stress reaching its maximum at the external surface of the barrel.

Due to the very high pressure required, the process of Hydraulic Autofrettage is slow, dangerous, and expensive. Consequently, in the early 1960's Davidson et al. [9] suggested a new process: Swage Autofrettage. In this process overstraining is accomplished by pushing an oversized tungsten carbide mandrel through the tube's blank, using a solid steel ram. This faster, safer, and cheaper process has been widely used since its introduction in gun barrel manufacturing, as well as in many other industries. Until recently [10,11], the two processes were considered to yield the same

pressure carrying capacity, provided the tube was overstrained to the same level. However, the factual data, accumulated mainly by the gun barrel industry, identified the clear advantages of Swage autofrettage over Hydraulic autofrettage in creating a higher residual hoop stress at the bore, and thus, further increasing the tubes pressure carrying capacity and extending the barrel's fatigue life.

The residual stress field induced by autofrettage serves as the key input to the stress analysis of both the intact and the cracked tubes. In spite of the fact that the two types of autofrettage have been in use for many years, the evaluation of their RSFs is complicated because of detailed elasto-plastic characteristics of the tube's material. Furthermore, while a two dimensional analysis proves satisfactory for Hydraulic autofrettage, Swage autofrettage necessitates a 3-D analysis to account for the three dimensionality of the process.

Many attempts have been made by e.g., [1,11–18] to calculate the RSF due to Hydraulic and Swage autofrettage. However, only in the last decade Perl and Perry [19,20] suggested a comprehensive 3-D model which enables an accurate evaluation of both Hydraulic and Swage autofrettage RSFs. This innovative model, is totally based on the experimentally measured stress-strain curve under repeated reversed loading, thus enabling an accurate characterization of the material's behavior including the Bauschinger effect in both tension and compression.

Once the material's characteristics of Cr-Ni-Mo-V modern gun barrel steel (a modified AISI 4340) are experimentally determined, the new model is applied to evaluate the hoop residual stress component for Hydraulic, Swage and Hill's autofrettage for a partially ($\varepsilon = 40\%$, 70%) or fully (100%) overstrained barrel presented in Fig. 1.

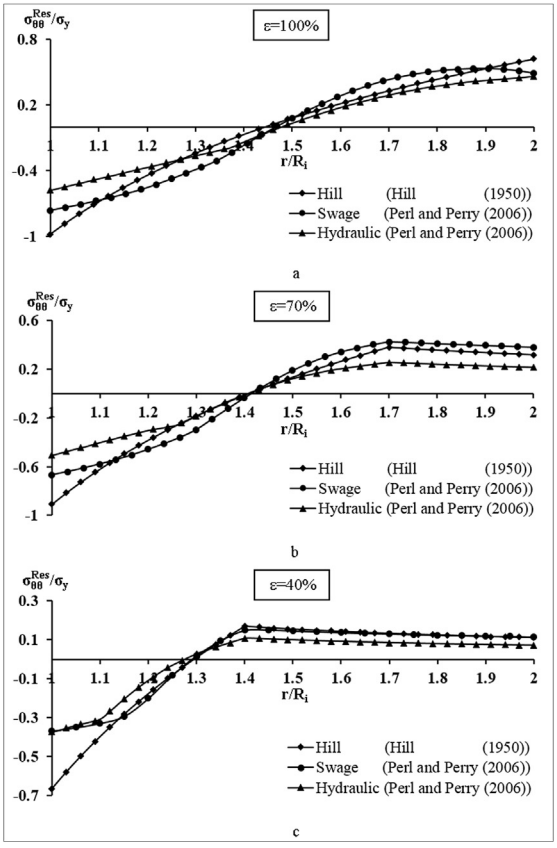

Fig. 1. The distribution of the residual hoop stress component for Hydraulic, Swage and Hill's autofrettage in a partially or fully overstrained barrel of $R_o/R_i = 2$ (a) $\varepsilon = 100\%$, (b) $\varepsilon = 70\%$, and (c) $\varepsilon = 40\%$.

The hoop residual stress (Fig. 1) is compressive at the inner portion of the barrel's wall and becomes tensile at its outer part. High internal pressure is applied to the barrel during the firing process creating a tensile hoop stress through the barrel's wall with a maximum at the bore and a minimum at the outer surface of the tube. When the residual stresses are superimposed on the stresses due to internal pressure, the compressive residual hoop stress $\sigma_{\theta\theta}^{Res}$ proves beneficial as it reduces the effective hoop stress at the inner portion of the barrel. The tensile part of the residual stress however, is detrimental as it increases the hoop stress at the outer part of the tube. Tables 1 and 2 respectively represent the values of the residual hoop stress at the inner and the outer surfaces of the tube, for the three types of autofrettage.

The largest differences between the RSFs of the three types of autofrettage occur at the inner and the outer surfaces of the barrel's wall. When considering the bore of a fully autofrettaged barrel (Fig. 1(a)), Hill's model predicts the highest negative $\sigma_{\theta\theta}^{Res}$ at the bore. The realistic $\sigma_{\theta\theta}^{Res}$ at the bore due to Swage and Hydraulic autofrettage is 22% smaller in absolute value for the former, and 41% for the latter than Hill's. This discrepancy results from the decrease in yield stress in compression due to the Bauschinger effect which is accounted for by the new model [19,20], while ignored by Hill's. Furthermore, in both autofrettage processes, upon unloading the barrel, re-yielding may occur at its inner wall, resulting in a further decrease in the yield stress. The differences in $\sigma_{\theta\theta}^{Res}$ near the bore between the three RSFs have a major impact on the fatigue life of the barrel. Higher negative $\sigma_{\theta\theta}^{Res}$ reduces the susceptibility to crack initiation and slows down crack growth rate, yielding a longer fatigue life. Whereas realistic fatigue lives for the barrel are yielded by Swage and Hydraulic autofrettage, Hill's "ideal" model highly overestimates its value.

When considering the outer surface of a fully autofrettaged barrel, Hill's model predicts the highest positive $\sigma_{\theta\theta}^{Res}$ (Fig. 1(a)). The realistic $\sigma_{\theta\theta}^{Res}$ at the outer surface of the barrel due to Swage and Hydraulic autofrettage is 21% and 26% smaller in value than Hill's respectively. Lower positive $\sigma_{\theta\theta}^{Res}$ decreases the sensitivity to external cracking and slows down crack growth rate. Hill's model considerably underestimates fatigue life in this case, while Swage

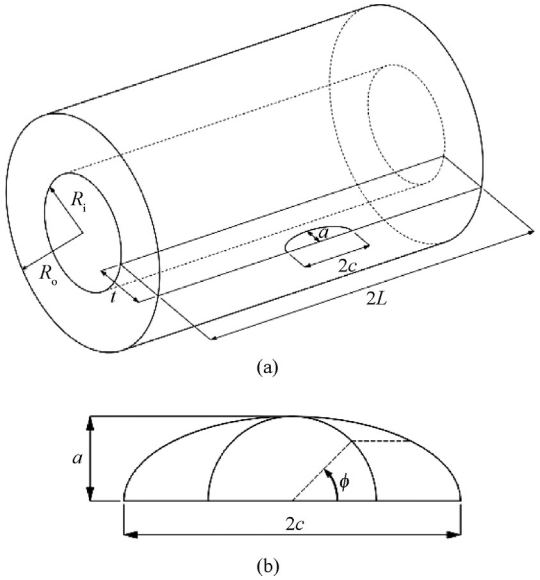

Fig. 2. (a) The cylinder with one external crack. (b) The parametric angle ϕ defining the points on the crack front.

Table 1
The relative residual hoop stress $\sigma_{\theta\theta}^{Res}/\sigma_y$ at the inner surface of the barrel $\boldsymbol{r}=\boldsymbol{R_i}$.

	$\sigma_{\theta\theta}^{Res}/\sigma_y$		
	Hill's autofrettage	Swage autofrettage	Hydraulic autofrettage
$\varepsilon=100\%$	−0.9796	−0.7638	−0.5795
$\varepsilon=70\%$	−0.9065	−0.6671	−0.5060
$\varepsilon=40\%$	−0.6666	−0.3694	−0.3744

Table 2
The relative residual hoop stress $\sigma_{\theta\theta}^{Res}/\sigma_y$ at the outer surface of the barrel $\boldsymbol{r}=\boldsymbol{R_o}$.

	$\sigma_{\theta\theta}^{Res}/\sigma_y$		
	Hill's autofrettage	Swage autofrettage	Hydraulic autofrettage
$\varepsilon=100\%$	0.6211	0.4890	0.4596
$\varepsilon=70\%$	0.3190	0.3817	0.2145
$\varepsilon=40\%$	0.1104	0.1143	0.0708

and Hydraulic autofrettage types yield realistic fatigue lives for the barrel.

At the inner portion of a partially autofrettaged barrel ($\boldsymbol{\varepsilon}=60\%$–80%), the patterns of the three RSFs are similar to that of the fully autofrettaged tube, though getting lower in absolute magnitude as the level of autofrettage decreases (cf. Fig. 1(b) and (c) to Fig. 1(a)). At the outer portion of a partially autofrettaged barrel, the RSF is different in both pattern and magnitude than in the case of full autofrettage. The magnitude of all RSFs decreases as the level of autofrettage decreases as can be anticipated. Furthermore, in the case of $\boldsymbol{\varepsilon}=70\%$ (Fig. 1(b), and Table 2), Swage autofrettage predicts the largest positive $\sigma_{\theta\theta}^{Res}$, while Hydraulic autofrettage predicts the smallest one, with an intermediate value for Hill's RSF. Hill's and Hydraulic autofrettage RSFs are 16% and 44% lower than Swage $\sigma_{\theta\theta}^{Res}$ respectively. In the case of $\boldsymbol{\varepsilon}=40\%$ (Fig. 1(c), and Table 2), Swage and Hill's autofrettage RSF are practically identical, while $\sigma_{\theta\theta}^{Res}$, due to Hydraulic autofrettage, is 38% lower.

The discrete values of RSF distribution are incorporated in the FE analysis in each case, using an equivalent temperature field which emulates them very accurately. The discrete values of the equivalent temperature field are calculated using the general algorithm developed by Perl [21]. A detailed description of obtaining the equivalent temperature field and its embodiment in the FE analysis is given in Perl [21]. In all the cases herein treated, the RSFs resulting from the equivalent temperature field are compared to the original RSFs and are all found to be practically identical.

3. Three dimensional analysis

The three dimensional analysis of the externally cracked barrel is based on Linear Elastic Fracture Mechanics (LEFM). The tube is modeled as an elastic cylinder of inner radius $\boldsymbol{R_i}$, outer radius $\boldsymbol{R_o}$, and wall thickness $\boldsymbol{t}$ ($\boldsymbol{R_o/R_i}=2$, and $\boldsymbol{t}=\boldsymbol{R_i}$) and length, $2\boldsymbol{L}$. The cylinder contains an external radial semi-elliptical crack of length $\boldsymbol{2c}$ and depth $\boldsymbol{a}$. The cylinder containing one crack is presented in Fig. 2(a). In order to avoid end effects, the ratio of the cylinder's length to its inner radius, $\boldsymbol{L/R_i}$, is taken to be at least as 4. The barrel is assumed to be made of a typical Cr-Ni-Mo-V barrel steel (a modified AISI 4340) with an initial yield stress of $\boldsymbol{\sigma_y}=1050$ MPa, Young modulus $\boldsymbol{E}=203$ GPa and Poisson's ratio $\boldsymbol{\nu}=0.3$. As a modern tank gun is considered, the internal pressure is set to be $\boldsymbol{p}=608$ MPa. All the SIFs are calculated by two methods: the displacement extrapolation method (DEM) and the J-integral. In the case of very shallow cracks of $\boldsymbol{a/t}=0.005$, SIFs are calculated along the crack front at intervals of $\boldsymbol{\Delta\phi}=3.6°$ for cracks of $\boldsymbol{a/c}\geq 0.4$, and at intervals of $\boldsymbol{\Delta\phi}=2.25°$ for cracks of $\boldsymbol{a/c}=0.2$. For deeper cracks, $\boldsymbol{a/t}\geq 0.01$, SIFs are calculated along the crack front at intervals of $\boldsymbol{\Delta\phi}=1.8°$ for cracks of $\boldsymbol{a/c}\geq 0.4$, and at intervals of $\boldsymbol{\Delta\phi}=1.125°$ for cracks of $\boldsymbol{a/c}=0.2$.

4. The finite element model

Because of its many symmetries only a quarter of the cylinder is analyzed (see Fig. 2(a)). The autofrettage RSF is induced in the FE model by an equivalent temperature field as previously explained. The model is solved using the commercial ANSYS 13.0 FE code [22]. To accommodate the singular stress field in the vicinity of the crack front, this area is covered with a layer of 20-node isoparametric brick elements collapsed to wedges, forming singular elements at the crack front [23]. On top of this layer, at least four additional layers, consisting of 20-node isoparametric brick elements, are meshed (see [2]). The rest of the model is divided into two zones. Zone I, the first quarter of the cylinder's length near the crack, is meshed with tetrahedron elements, while Zone II, the rest of the cylinder is meshed with brick elements. Near the crack front, the elements are chosen to be small, and their size is gradually increased when moving away from the crack. SIFs are extracted using two methods built into ANSYS: The J-integral [24], and the crack-face displacement extrapolation method. SIFs are calculated at equally spaced discrete points along the crack front.

4.1. Validation of the FE model

Since presently there are no values for $\boldsymbol{K_{IA}}$ for external cracks in autofrettaged cylinders, the FE model is firstly validated by calculating $\boldsymbol{K_{IP}}$ distribution along a semi-circular external crack of depth $\boldsymbol{a/t}=0.1$, and comparing it with the results obtained in API 579-1 [25] using the weight function method. The results presented in Fig. 3 show that the present and API 579-1 results are within less than 1% except for the external surface point ($\boldsymbol{\phi}=0°$) where they differ by about 4.5%. In order to further validate the model, $\boldsymbol{K_{IA}}$ distribution along the front of a semi-circular external crack of depth $\boldsymbol{a/t}=0.1$ prevailing in a fully autofrettaged cylinder is evaluated by two independent methods: The J-integral method and the displacement extrapolation procedure, which then are compared to each other in Fig. 4. The maximal difference of about 1.5% between the two methods occurs at $\boldsymbol{\phi}=0°$, at the intersection of the crack plane with the outer surface of the cylinder. As one moves away from this point, the difference in $\boldsymbol{K_{IA}/K_{00}}$ drops to about 0.2%.

In order to maintain high accuracy of the evaluated SIFs, convergence tests were conducted for $\boldsymbol{K_{IA}}$. The value of $\boldsymbol{K_{IA}/K_{00}}$ at the deepest point ($\boldsymbol{\phi}=90°$) of a semi-circular crack of depth $\boldsymbol{a/t}=0.1$ served as a convergence criterion. $\boldsymbol{K_{IA}/K_{00}}$ was evaluated for a fully autofrettaged (Hill's model) barrel. Fig. 5 represents the convergence of $\boldsymbol{K_{IA}/K_{00}}$ as a function of the number of DOF. The results indicate that above 1,200,000 DOF, the error is less than

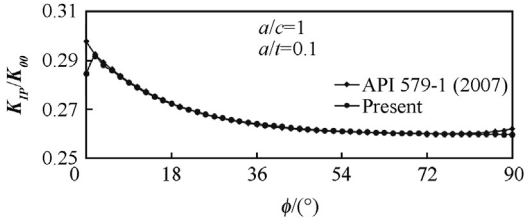

Fig. 3. A comparison between the present distribution of $\boldsymbol{K_{IP}/K_{00}}$ along the front of a semi-circular external crack of depth $\boldsymbol{a/t}=0.1$, in a fully autofrettaged barrel of $\boldsymbol{R_o/R_i}=2$ evaluated by the DEM method and those of API 579-1 [25] evaluated by the weight function method.

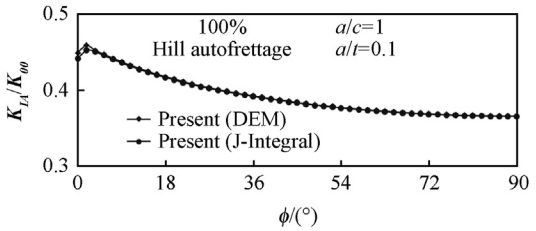

Fig. 4. A comparison between the distribution of K_{IA}/K_{00} along the front of a semi-circular, external crack of depth $a/t = 0.1$, in a barrel of $R_o/R_i = 2$ evaluated by the displacement extrapolation method (DEM) and the one obtained by the J-integral.

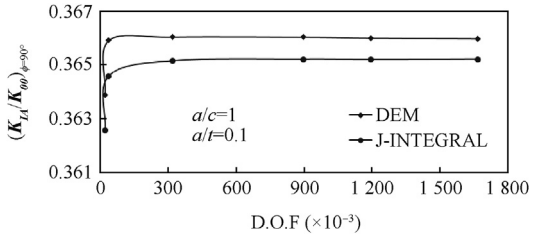

Fig. 5. $K_{IA}/K_{00(\phi=90^\circ)}$ as a function of the number of DOF for a semi-circular, $a/c = 1$, external crack of depth $a/t = 0.1$, in a fully autofrettaged barrel of $R_o/R_i = 2$.

0.02%. Thus, in order to ensure high accuracy, 1,600,000 DOF are employed for all cases.

5. Numerical results and discussion

Unlike the case of an internal crack, where K_{IA} is usually negative reducing the effective SIF, in the case of external cracks, K_{IA} values are usually positive, therefore, increasing the effective SIF which has a disadvantageous effect on the barrel's fatigue life. In the present analysis K_{IA} values are calculated for external radial cracks prevailing in a typical barrel of radii ratio $R_o/R_i = 2$ for a wide range of relevant crack depth to wall-thickness ratios $a/t = 0.005$, 0.01, 0.04, 0.07, and 0.1, for various crack ellipticities $a/c = 0.2$, 0.4, 0.6, 0.8, and 1.0, and for five levels of Swage, Hydraulic and Hill's autofrettage of $\varepsilon = 40\%$, 60%, 70%, 80%, and 100%. In total, 375 different 3-D external crack cases are analyzed. In order to enable future comparison and superposition, the SIFs K_{IA} and K_{IP} are normalized further on, with respect to:

$$K_{00} = p\sqrt{R_i} \tag{1}$$

5.1. K_{IA} distribution along an external-crack's front in a fully autofrettaged barrel

K_{IA} values for all crack configurations in a fully autofrettaged gun barrel are calculated for Hydraulic, Swage and Hill's autofrettage RSFs and are normalized with respect to K_{00}. In the analysis to follow, K_{IA} distributions along the crack front are separately presented for semi-circular cracks $a/c = 1.0$ and for semi-elliptical ones $a/c < 1.0$.

5.1.1. Semi-circular cracks $a/c = 1.0$

Typical distributions of K_{IA}/K_{00} along the crack front of an external semi-circular crack of depth $a/t = 0.005$ and 0.1, prevailing in a fully autofrettaged barrel are presented in Figs. 6 and 7 respectively. Generally speaking, there are two patterns of K_{IA}/K_{00} distributions. The first one has its maximum at $\phi = 0^\circ$ and its minimum at $\phi = 90^\circ$. This type of distribution occurs in the cases of

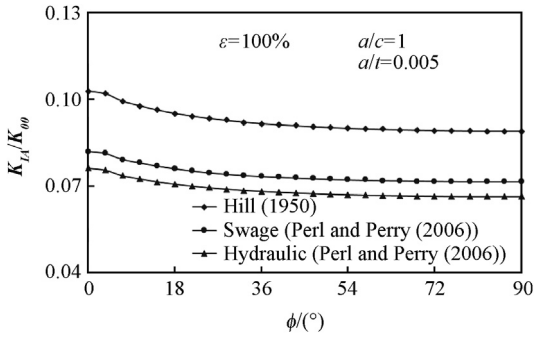

Fig. 6. K_{IA}/K_{00} vs. ϕ along the front of a semi-circular crack of depth $a/t = 0.005$. in a fully autofrettaged cylinder.

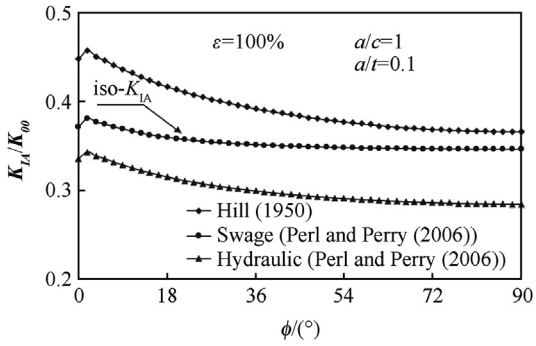

Fig. 7. K_{IA}/K_{00} vs. ϕ along the front of a semi-circular crack of depth $a/t = 0.1$ in a fully autofrettaged cylinder.

Hydraulic and Hill's autofrettage for cracks of depths $a/t = 0.005$ and 0.1, and only for shallow cracks $a/t = 0.005$ in the case of Swage autofrettage (see Figs. 6 and 7). The second distribution pattern is coined Iso- K_{IA} as the distribution is almost even along the crack front. This distribution is characteristic only of deep cracks, e.g., $a/t = 0.1$, in the case of Swage autofrettage (see Fig. 7).

From Figs. 6 and 7 it is evident that the magnitude of K_{IA} differs considerably between the three types of autofrettage: Hill's yielding the highest K_{IA} value, Swage autofrettage predicting an intermediate value, and Hydraulic autofrettage producing the lowest K_{IA}. These results have a direct impact on the effective SIF and thus on the fatigue life of the barrel. In this case Hill's "ideal" RSF excessively and non-realistically underestimate the total fatigue life of the barrel.

Table 3 summarizes the ratios between the maximum values of these distributions, which occur at $\phi = 0^\circ$, for the five crack depths herein evaluated. The ratios between the magnitudes of the maximum SIF due to the three types of autofrettage are practically crack depth independent. On the average in this case, Swage and Hydraulic autofrettage produce SIFs which are about -19% and 26% lower than Hill's respectively.

5.1.2. Semi elliptical cracks $a/c < 1.0$

The distribution of K_{IA}/K_{00} along the crack front of an external radial crack of $a/c < 1.0$ is ellipticity dependent:

5.1.2.1. Cracks of ellipticity $1.0 > a/c > 0.8$. When crack ellipticity is larger than $a/c = 0.8$, K_{IA}/K_{00}, distributions along the crack front have a similar pattern to that of semi-circular cracks (as in Figs. 6 and 7), bearing their maximal values near the outer surface of the barrel.

Table 3
K_{IAmax} for full Swage and Hydraulic autofrettage relative to Hill's solution for semi-circular external cracks of various depths.

Relative maximal SIF at $\phi = 0°$	Relative crack depth for a/c=1.0				
	$a/t = 0.005$	$a/t = 0.01$	$a/t = 0.04$	$a/t = 0.07$	$a/t = 0.1$
$K^{Swage}_{IAmax}/K^{Hill}_{IAmax}$	0.80	0.80	0.81	0.82	0.83
$K^{Hyd}_{IAmax}/K^{Hill}_{IAmax}$	0.74	0.74	0.74	0.75	0.75

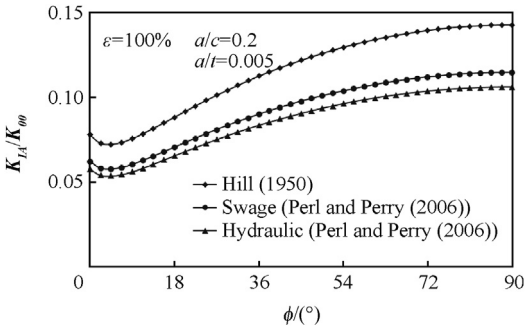

Fig. 8. K_{IA}/K_{00} vs. ϕ along the front of a slender semi-elliptical external crack. of $a/c = 0.2$ and depth $a/t = 0.005$ in a fully autofrettaged cylinder.

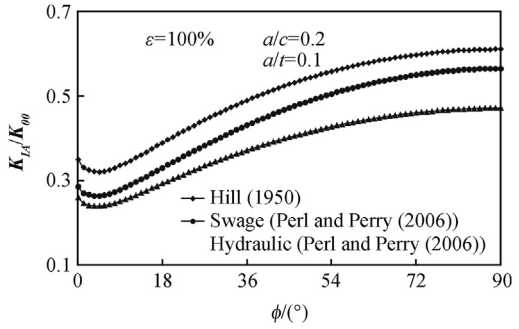

Fig. 9. K_{IA}/K_{00} vs. ϕ along the front of a slender semi-elliptical external crack. of $a/c = 0.2$ and depth $a/t = 0.1$ in a fully autofrettaged cylinder.

5.1.2.2. Cracks of ellipticity $0.6 > a/c \geq 0.2$. Typical distributions of K_{IA}/K_{00} for slender cracks are presented in Figs. 8 and 9 for a crack of ellipticity $a/c = 0.2$ and depths $a/t = 0.005$ and 0.1 respectively. The maximum value for both cracks occurs at $\phi = 90°$, the deepest point of the crack., and the relations between K_{IA}/K_{00} values for the three autofrettage types presented in Table 4, are practically crack depth independent and are almost identical to those presented in Table 3 i.e., $K^{Swage}_{IAmax}/K^{Hill}_{IAmax} \approx 0.81$ and $K^{Hyd}_{IAmax}/K^{Hill}_{IAmax} \approx 0.74$.

5.1.2.3. Cracks of ellipticity $1.0 \geq a/c \geq 0.6$. In this range of ellipticities, as the one presented in Figs. 10 and 11, cracks are ***iso-K_I*** cracks, having an almost uniform distribution of K_{IA}/K_{00} around the entire crack front. The more crack ellipticity deviates from the ***iso-K_I*** range, the higher the non-uniformity of K_{IA}/K_{00} distribution along the crack front as can be seen, for example, in Fig. 12 for the three types of autofrettage and $\varepsilon = 100\%$. Based on the present results, cracks can be considered as "***iso-cracks***" for Hill's autofrettage in the range of ellipticities of $0.8 \geq a/c \geq 0.6$, for Hydraulic autofrettage $0.8 \geq a/c \geq 0.7$ and for Swage autofrettage $1.0 \geq a/c \geq 0.8$.

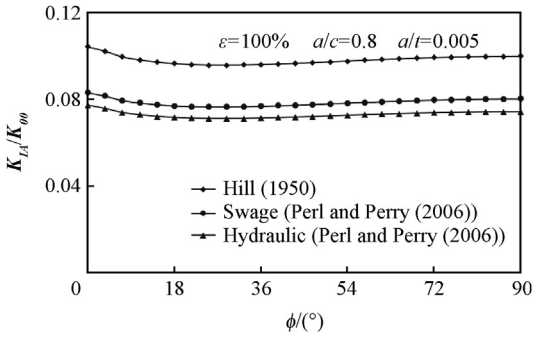

Fig. 10. K_{IA}/K_{00} vs. ϕ along the front of an iso-semi-elliptical crack of $a/c = 0.8$ and depth $a/t = 0.005$ in a fully autofrettaged cylinder.

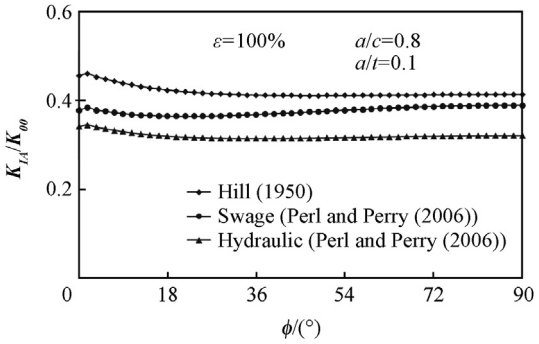

Fig. 11. K_{IA}/K_{00} vs. ϕ along the front of an iso-semi-elliptical crack of $a/c = 0.8$ and depth $a/t = 0.1$ in a fully autofrettaged cylinder.

5.2. K_{IA} distribution along an external-crack's front in a partially autofrettaged barrel

Most gun barrels are commonly only partially autofrettaged to about $\varepsilon = 70\%$, since the marginal benefit in increasing the level of autofrettage from $\varepsilon = 70\%$ to $\varepsilon = 100\%$ is about 10–15% [2] in augmenting the allowable internal pressure. However, this increase in the level of autofrettage has a major disadvantage of enhancing

Table 4
K_{IAmax} for full Swage and Hydraulic autofrettage relative to Hill's solution for semi-elliptical external cracks of $a/c = 0.2$ for various crack depths.

Relative maximal SIF at $\phi = 90°$	Relative crack depth for $a/c = 0.2$				
	$a/t = 0.005$	$a/t = 0.01$	$a/t = 0.04$	$a/t = 0.07$	$a/t = 0.1$
$K^{Swage}_{IAmax}/K^{Hill}_{IAmax}$	0.80	0.80	0.81	0.81	0.82
$K^{Hyd}_{IAmax}/K^{Hill}_{IAmax}$	0.74	0.74	0.74	0.74	0.75

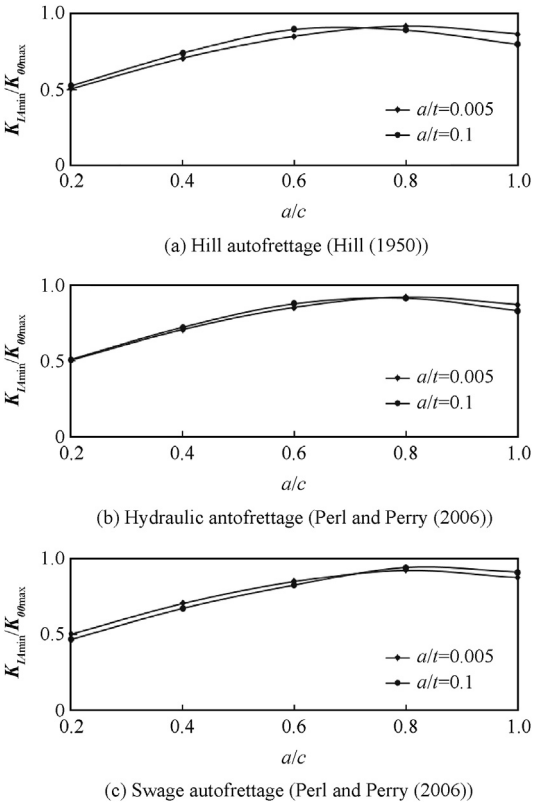

Fig. 12. The non-uniformity of K_{IA} distribution along the crack front vs. crack ellipticity for the three types of autofrettage and $\varepsilon = 100\%$.

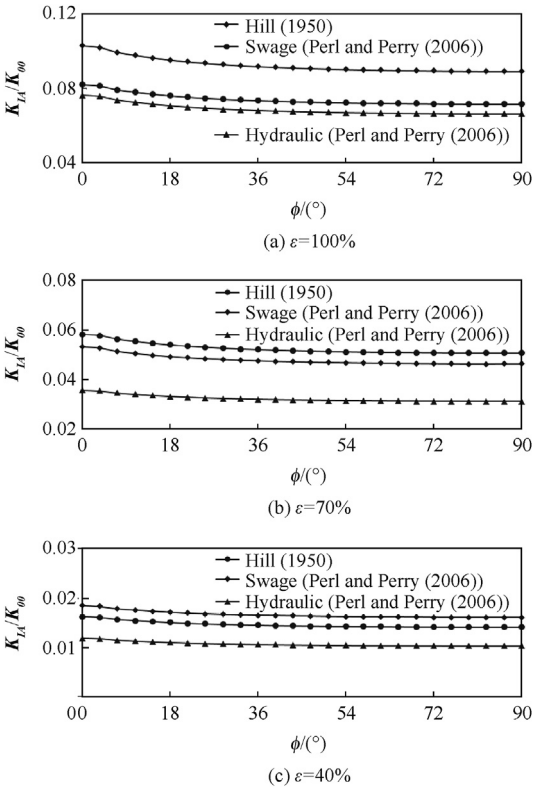

Fig. 13. K_{IA}/K_{00} vs. ϕ for an external radial semi-circular crack of depth $a/t = 0.005$ prevailing in a barrel overstrained to three different levels of Hill's, Swage and Hydraulic autofrettage: $\varepsilon = 100\%$, 70%, and 40%.

Table 5
Values of K_{IAmax} for an external crack in a partially autofrettaged barrel ($\varepsilon = 70\%$, 60%, 40%) relative to a fully overstrained tube for the three types of autofrettage.

Relative maximal SIF	Type of Autofrettage		
	Hill	Swage	Hydraulic
$\frac{K_{IAmax}\ (\varepsilon = 70\%)}{K_{IAmax}(\varepsilon = 100\%)}$	0.56	0.71	0.50
$\frac{K_{IAmax}\ (\varepsilon = 60\%)}{K_{IAmax}(\varepsilon = 100\%)}$	0.40	0.59	0.36
$\frac{K_{IAmax}\ (\varepsilon = 40\%)}{K_{IAmax}(\varepsilon = 100\%)}$	0.19	0.20	0.16

external cracking of the barrel. A second reason for investigating the influence of partial autofrettage is the fact that during the barrel's life the residual stress field due to autofrettage deteriorates, resulting in a lower overstrain level, which in turn affects its fatigue life.

Fig. 13(a–c) represents K_{IA}/K_{00} for an external radial semi-circular crack of depth $a/t = 0.005$ prevailing in a barrel overstrained to three different levels of Hill's, Swage and Hydraulic autofrettage: $\varepsilon = 100\%$, 70%, and 40%. As anticipated, the value of K_{IA} decreases as the level of autofrettage decreases. The relative values of K_{IAmax} for $\varepsilon = 70\%$, 60%, and 40% with respect to $\varepsilon = 100\%$ for the three types of autofrettage are given in Table 5.

From Table 5 it can be seen that lowering the level of autofrettage from $\varepsilon = 100\%$ to $\varepsilon = 70\%$ reduces considerably the detrimental effect on an external crack by about 30% for Swage autofrettage and 50% for hydraulic autofrettage.

6. Concluding remarks

The distributions of K_{IA} along the front of a single external radial crack in an overstrained smooth gun barrel are evaluated for numerous crack configurations evaluating the effects of the type and level of autofrettage and of the crack's geometry. K_{IA} values are evaluated for three types of autofrettage: Swage, Hydraulic and Hill's, for five levels of overstraining $\varepsilon = 40\%$, 60%, 70%, 80%, and 100%, for crack depths of $a/t = 0.005$, 0.01, 0.04, 0.07, and 0.1, and for various crack ellipticities $a/c = 0.2$, 0.4, 0.6, 0.8, and 1.0.

In spite of the fact that all types of autofrettage herein discussed have an adverse effect on external cracks, they differ considerably in the magnitude of this negative effect. The detrimental effect of both Hydraulic and Swage autofrettage on the external cracking of a ***fully autofrettaged*** gun barrel is found to be much smaller than that anticipated by Hill's "ideal" autofrettage. This results from the fact that Hill's RSF ignores the Bauschinger effect. The incorporation of the Bauschinger effect in the cases of Swage and Hydraulic autofrettage results in a substantial reduction of the material's yield stress and thus, considerably reducing K_{IA} values.

In the case of partial autofrettage, the detrimental effect of the three RSFs is somewhat different. All three RSFs become weaker as the level of autofrettage decreases, having a less severe detrimental effect on the barrel's life. In the case of 70% overstraining, Swage autofrettage has a 78% higher detrimental effect than Hydraulic autofrettage, while for $\varepsilon = 40\%$, the adverse effect of Swage overstraining is 61% higher than that of Hydraulic overstraining.

Reducing the level of Swage and Hydraulic overstraining from $\varepsilon = 100\%$ to $\varepsilon = 70\%$ has only a marginal effect on the barrel's pressure capacity and on the beneficial effect on internal cracking. However, it considerably reduces the unfavorable effect on external cracking.

The evaluation of the combined effect of overstraining and pressurization of the barrel on external cracking is presently underway. The combined SIFs $K_{IN} = K_{IP} + K_{IA}$ are to be determined

as well as the maximum value K_{INmax} which controls fracture processes. The results of this study will be presented elsewhere.

References

[1] Hill R. The mathematical theory of plasticity. New York: Oxford University Press; 1950.
[2] Perl M, Saley T. Swage and hydraulic autofrettage impact on fracture endurance and fatigue life of an internally cracked smooth gun barrel Part I - the effect of overstraining. Eng Fract Mech 2017;182:372–85.
[3] Perl M, Saley T. Swage and hydraulic autofrettage impact on fracture endurance and fatigue life of an internally cracked smooth gun barrel Part II- the combined effect of pressure and overstraining. Eng Fract Mech 2017;182:386–99.
[4] Raju IS, Newman JC. Stress-intensity factors for internal and external surface cracks in cylindrical vessels. J Press Vessel Technol Trans ASME 1982;104:293–8.
[5] Zheng XJ, Kiciak A, Glinka G. Weight function and stress intensity factors for internal surface semi-elliptical crack in thick-walled cylinder. Eng Fract Mech 1997;58(3):207–21.
[6] Anderson TL, et al. Development of stress intensity factor solutions for surface and embedded cracks in API 579. New York, NY: Welding Research Council, Inc.; 2002. Bulletin 471.
[7] Gerasimenko A. Stress intensity factors of external surface cracks in a vertical cylindrical steel tank. Mod Appl Sci 2014;8(6).
[8] Jacob L. La Résistance et L'équilibre Élastique des Tubes Frettés", Memorial de L'artillerie Navale, 1; 1907. p. 43–155.
[9] Davidson TE, Barton CS, Reiner AN, Kendall DP. A new approach to the autofrettage of high strength cylinders. Experimental Mechanics; 1962. p. 33–40.
[10] Benet R, E Laboratories. Autofrettage design manual of gun tubes. N.Y: Watervliet Arsenal; 1970.
[11] Parker AP, O'Hara GP, Underwood JH. Hydraulic versus swage autofrettage and implications of the Bauschinger effect. ASME J Press Vessel Technol 2003;125:309–14.
[12] Davidson TE, Kendall DP, Reiner AN. Residual stresses in thick-walled cylinders resulting from mechanically induced overstrain. Exp Mech 1963;3:253–62.
[13] Chen PCT. Numerical prediction of residual stress in an autofrettage tube of compressible material. In: Proceedings of the 1981 army numerical analysis and computer conference; 1981. p. 315–62.
[14] Jahed H, Dubey RN. An axisymmetric method of elastic-plastic analysis capable of predicting residual stress field. J Press Vessel Technol 1997;119:264–73.
[15] Parker AP. Autofrettage of open-end tubes-pressures, stresses, strains, and code comparisons. ASME J Press Vessel Technol 2001;123:271–81.
[16] Perry J, Aboudi J. Elasto-plastic stresses in thick walled cylinders. ASME J Press Vessel Technol 2003;125:248–52.
[17] Ironmonger MJ. A numerical study of swage autofrettage. ASME J Press Vessel Technol 2003;125:347–51.
[18] Huang X. A general autofrettage model of a thick-walled cylinder based on tensile- compressive stress-strain curve of a material. J Strain Anal Eng Des 2005;40(6):599–608.
[19] Perl M, Perry J. "An experimental-numerical determination of the three dimensional autofrettage residual stress field incorporating Bauschinger effect. ASME J Press Vessel Technol 2006;128:173–8.
[20] Perry J, Perl M. A 3-D model for evaluating the residual stress field due to swage autofrettage. Trans ASME J Press Vessel Technol 2008;130:041211 (6 pages).
[21] Perl M. The temperature field for simulating partial autofrettage in an elasto-plastic thick-walled cylinder. Trans ASME J Press Vessel Technol 1988;110:100–2.
[22] ANSYS release 13.0. Canonsburg, PA 15317, USA: ANSYS Inc.; 2010.
[23] Barsom RS. On the use of isoparametric finite elements in linear fracture mechanics. Int J Numer Methods Eng 1976;10(1):25–37.
[24] Rice JR. A path independent integral and the approximate analysis of strain concentration by notched and cracks. J Appl Math 1968;35:379–86.
[25] API 579-1. second ed. 2007. ASME FFS-1 Fitness-For-Service.